



Cite this: *Dalton Trans.*, 2024, **53**, 3675

Coordination recognition of differential template units of lanthanide chiral chain†

Wen-Wen Qin,[‡] Bing-Fan Long,[‡] Zhong-Hong Zhu,[†] * Hai-Ling Wang, Fu-Pei Liang* and Hua-Hong Zou[†] *

Coordination-driven self-assembly processes often produce remarkable structures. In particular, self-assembly processes mediated by chiral template units have provided research ideas for analyzing the formation of chiral macromolecules in living organisms. In this study, by regulating the proportion of reaction raw materials in the “one-pot” synthesis of lanthanide complexes, we constructed chiral template units with different coordination orientations. As a result, lanthanide chiral chains connected to different structures were obtained through the self-assembly process of coordination recognition. In particular, driven by coordination, chiral template units with codirectional coordination points (called *cis* configuration) coordinate solely with *cis* template units during the self-assembly process to obtain a one-dimensional (1D) chain **R-1/S-1** with an “S”-shaped distribution. Moreover, chiral template units with reversed coordination sites (called *trans* configuration) and twisted chiral template units are connected solely to templates with the same configuration to form a 1D chain **R-2/S-2** with an axial helix. A circular dichroism spectrum shows that **R-1/S-1** and **R-2/S-2** are two pairs of enantiomers. The controllable construction of these two differential 1D chains is of great significance for studying coordination recognition at the molecular level. To the best of our knowledge, this is the first study to construct a 1D lanthanide chain through the self-assembly process of coordination recognition. The assembly process of nucleotides to form a hierarchical structure is simulated. This work provides a vivid example of the controllable synthesis of lanthanide complexes with precise structures and offers a new perspective on the formation process of chiral macromolecules that simulates natural processes.

Received 2nd December 2023,
Accepted 25th January 2024

DOI: 10.1039/d3dt04028c

rsc.li/dalton

Introduction

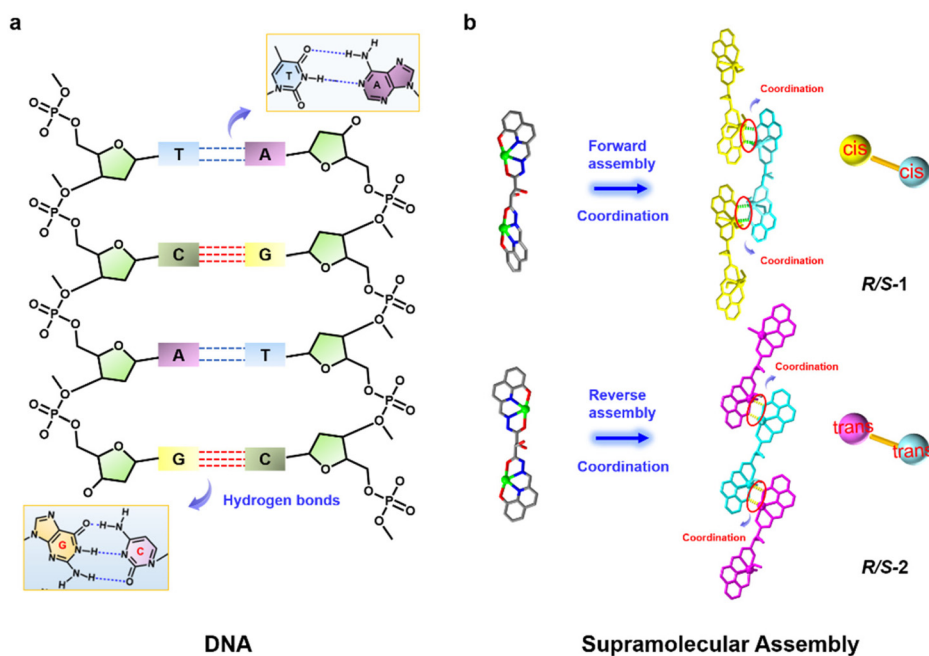
Chirality is a basic material property that exists in nature and plays a vital role in various living systems.^{1–3} Proteins, polysaccharides, and nucleic acids in living organisms are chiral compounds synthesized from optically pure structural units, and several essential life activities involve highly enantioselective processes.^{4–6} Examples include converting L-amino acids into proteins with α -helices or D-nucleotides into DNA with P-helices (Scheme 1).⁷ The accurate construction of chiral molecules and in-depth study of the chiral interaction mechanisms among their structures can provide insights into the origin and transfer of chirality.^{8–11} However, chiral macro-

molecules in living systems are usually formed by simple chiral motifs undergoing complex reaction processes, and it is difficult to study these processes using existing methods. Therefore, there is an urgent need to develop a simple and effective model to facilitate the understanding of the formation process of chiral macromolecules.^{12–16} Coordination-driven self-assembly can simulate the self-recognition process among chiral template units of different configurations, providing new research ideas for simplifying and simulating the formation of complex chiral macromolecules having multilevel structures from simple primitives in living organisms.^{17–20} In addition, chiral lanthanide complexes show attractive application prospects in the fields of enantioresolution, molecular recognition, nonlinear optics and asymmetric catalysis. In 2017, Cui *et al.* reported a chiral porous octahedral cage that can serve as an efficient asymmetric supramolecular catalyst to achieve high catalytic activity and selectivity.²¹ In 2018, Tong *et al.* constructed an Er-based chiral SMM using the chiral ligand binaphthyl phosphate.²² In 2023, Kong *et al.* used amino acid amide groups and complexes of Ni³⁺ and lanthanide metals as basic building blocks to assemble into a DNA-like chiral double helix structure driven by coordination bonds

School of Chemistry and Pharmaceutical Sciences, State Key Laboratory for Chemistry and Molecular Engineering of Medicinal Resources, Guangxi Normal University, Guilin 541004, P. R. China. E-mail: 18317725515@163.com, liangfupei@glut.edu.cn, gxnuchem@foxmail.com

† Electronic supplementary information (ESI) available. CCDC 2306659, 2306660, 2306784 and 2306664. For ESI and crystallographic data in CIF or other electronic format see DOI: <https://doi.org/10.1039/d3dt04028c>

‡ These authors contributed equally to this work.

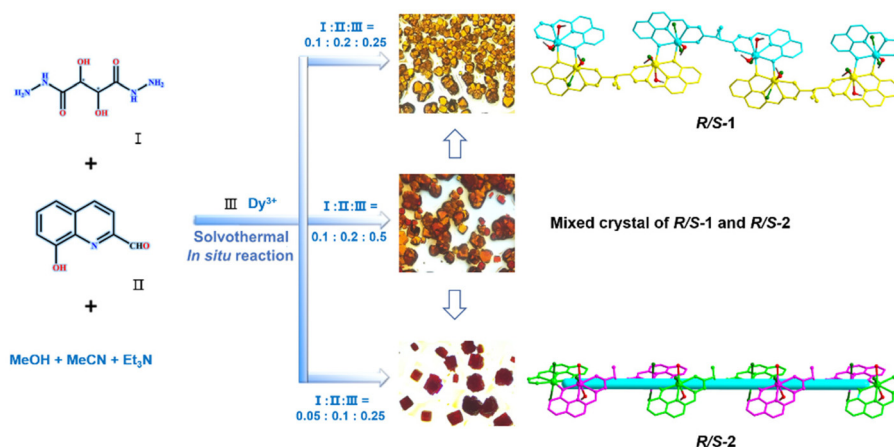


Scheme 1 (a) The recognition process between nucleic acid base pairs, (b) schematic diagram of coordination recognition assembly of complex fragments with different orientations.

and hydrogen bonds, achieving the goal of chirality transfer from microscopic to mesoscopic scales.¹⁷ The controllable preparation of chiral lanthanide complexes is extremely challenging due to the large ion radius, variable coordination number, diverse coordination modes, and easy distortion of the coordination sphere of lanthanide metals.^{23–29} Despite these difficulties, we have made some progress in the directional construction of chiral lanthanide clusters having specific shapes and structural connections and their self-assembly mechanisms.^{30,31} In 2022, we performed for the first time the directional construction of two chiral lanthanide clusters having different nucleus numbers by manipulating the ring growth mechanism and subsequently proposed a linear growth mechanism to construct linear hexanuclear chiral lanthanide clusters.^{18,19} To date, it is unknown whether chiral template primitives have considerable recognition ability for specific configurations during the self-assembly process. The selective recognition ability for specific configurations is crucial in analyzing chirality in living organisms and building an effective platform for research on simplifying the connection of chiral units to form complex chiral compounds.

Herein, we reacted *R/S*-tartaric acid dihydrazide (I), 8-hydroxyquinoline-2-carboxaldehyde (II), and $\text{DyCl}_3 \cdot 6\text{H}_2\text{O}$ (III) under heating conditions to obtain yellow and red mixed blocky crystals, ***R-1/S-1*** and ***R-2/S-2***, respectively. Notably, when other reaction conditions were kept constant and the ratio of the reaction raw materials was adjusted to I : II : III = 0.1 : 0.2 : 0.25, only pure yellow blocky crystals, ***R-1/S-1***, were obtained, whereas when the reaction raw materials were adjusted to I : II : III = 0.05 : 0.1 : 0.25, only pure red blocky crystals, ***R-2/S-2***,

were obtained (Scheme 2). The experimental results reveal that under the condition that two different configurations of template units simultaneously exist during the “one-pot” synthesis process, the chiral template units with codirectional coordination points (called *cis* configuration) or reversed coordination sites (called *trans* configuration) only selectively coordinate with the template units of the same configuration during coordination. This indicates that the chiral template unit has considerable selective recognition ability during the self-assembly process. In addition, by controlling the ratio of the reaction raw materials, the formation of chiral template units with different coordination orientations can be manipulated, and coordination recognition can be used to obtain pure ***R-1/S-1*** and ***R-2/S-2***. The recognition and assembly of chiral template units having different coordination orientations is similar to the specific recognition process between nucleic acid base pairs, providing insights into the formation process of complex chiral macromolecules (Scheme 1). Notably, this coordination-driven self-assembly process exhibits great potential for constructing the hierarchical structures of biological macromolecules and is of great importance for simplifying and simulating the formation process of complex chiral macromolecules at the supramolecular level. Furthermore, circular dichroism (CD) spectra confirmed the chirality of ***R-1/S-1*** and ***R-2/S-2*** and revealed that they are two pairs of enantiomers. To the best of our knowledge, this is the first study to construct chiral one-dimensional (1D) lanthanide chains through the self-assembly process of coordination recognition. This study provides a new idea for the directional, controllable, and precise synthesis of chiral lanthanide complexes, advancing



Scheme 2 Regulating reaction conditions controls the synthesis schematic of *R-1/S-1* and *R-2/S-2*.

the development of crystal engineering of lanthanide complexes with different structural connections. In addition, it offers a new perspective on simulating the formation process of complex chiral macromolecules in natural processes.

Experimental section

The synthesis method

Synthesis of $[[\text{Dy}_2(\text{R-L}^1)(\text{Cl})_3(\text{CH}_3\text{OH})_3]\cdot\text{Cl}\cdot 4\text{CH}_3\text{OH}\cdot\text{CH}_3\text{CN}\cdot 2\text{H}_2\text{O}]_n$ (*R-1*). *R*-Tartaric acid dihydrazide (0.1 mmol, 0.0178 g), 8-hydroxyquinoline-2-carboxaldehyde (0.2 mmol, 0.0346 g), $\text{DyCl}_3\cdot 6\text{H}_2\text{O}$ (0.25 mmol, 0.0942 g) and triethylamine (20 μL) were dissolved in mixed solvents of methanol (1.8 mL) and acetonitrile (0.2 mL) in a Pyrex tube. The tube was sealed and heated at 80 °C in an oven for 24 h, then cooled down slowly, yellow block crystals were obtained with a yield of about 26% (based on $\text{DyCl}_3\cdot 6\text{H}_2\text{O}$). Elemental analysis theoretical value ($\text{C}_{33}\text{H}_{53}\text{Cl}_4\text{Dy}_2\text{N}_7\text{O}_{15}$): C, 31.59%; H, 4.25%; N, 7.81%; experimental value: C, 31.63%; H, 4.22%; N, 7.74%. Infrared spectrum data (IR, KBr pellet, cm^{-1}): 3399(s), 1615(s), 1551(s), 1502(s), 1455(s), 1381(s), 1279(m), 1205(s), 1164(m), 1094(s), 1063(m), 955(w), 843(s), 736(m), 695(m), 599(w).

Synthesis of $[[\text{Dy}_2(\text{S-L}^1)(\text{Cl})_3(\text{CH}_3\text{OH})_3]\cdot\text{Cl}\cdot 6\text{CH}_3\text{OH}]_n$ (*S-1*). The synthesis method was similar to that for *R-1* by using *S*-tartaric acid dihydrazide instead of *R*-tartaric acid dihydrazide. The yield is 26% (based on $\text{DyCl}_3\cdot 6\text{H}_2\text{O}$). Elemental analysis theoretical value ($\text{C}_{33}\text{H}_{54}\text{Cl}_4\text{Dy}_2\text{N}_6\text{O}_{15}$): C, 31.92%; H, 4.38%; N, 6.76%; experimental value: C, 31.70%; H, 4.30%; N, 6.78%. Infrared spectrum data (IR, KBr pellet, cm^{-1}): 3397(s), 1619(s), 1550(s), 1503(s), 1455(s), 1381(s), 1273(m), 1203(s), 1164(m), 1090(s), 1066(m), 955(w), 843(s), 737(m), 697(w), 598(w).

Synthesis of $[[\text{Dy}_2(\text{R-L}^1)(\text{Cl})_3(\text{CH}_3\text{OH})_2]\cdot\text{Cl}\cdot\text{H}_2\text{O}\cdot 4\text{CH}_3\text{OH}]_n$ (*R-2*). *R*-Tartaric acid dihydrazide (0.05 mmol, 0.0089 g), 8-hydroxyquinoline-2-carboxaldehyde (0.1 mmol, 0.0173 g), $\text{DyCl}_3\cdot 6\text{H}_2\text{O}$ (0.25 mmol, 0.0942 g) and triethylamine (20 μL) were dissolved in mixed solvents of methanol (1.8 mL) and

acetonitrile (0.2 mL) in a Pyrex tube. The tube was sealed and heated at 80 °C in an oven for 24 h, then cooled down slowly, red block crystals were obtained with a yield of about 18% (based on $\text{DyCl}_3\cdot 6\text{H}_2\text{O}$). Elemental analysis theoretical value ($\text{C}_{30}\text{H}_{43}\text{Cl}_4\text{Dy}_2\text{N}_6\text{O}_{13}$): C, 30.96%; H, 3.81%; N, 7.22%; experimental value: C, 31.02%; H, 3.75%; N, 7.25%. Infrared spectrum data (IR, KBr pellet, cm^{-1}): 3400(s), 1620(s), 1550(w), 1504(s), 1435(s), 1387(s), 1279(m), 1197(w), 1096(s), 848(w), 792(w), 742(m), 594(m), 493(w).

Synthesis of $[[\text{Dy}_2(\text{S-L}^1)(\text{Cl})_3(\text{CH}_3\text{OH})_2]\cdot\text{Cl}\cdot 5\text{CH}_3\text{OH}]_n$ (*S-2*). The synthesis method was similar to that for *R-2* by using *S*-tartaric acid dihydrazide instead of *R*-tartaric acid dihydrazide. The yield is 18% (based on $\text{DyCl}_3\cdot 6\text{H}_2\text{O}$). Elemental analysis theoretical value ($\text{C}_{31}\text{H}_{45}\text{Cl}_4\text{Dy}_2\text{N}_6\text{O}_{13}$): C, 31.64%; H, 3.85%; N, 7.14%; experimental value: C, 31.67%; H, 3.82%; N, 7.10%. Infrared spectrum data (IR, KBr pellet, cm^{-1}): 3400(s), 1617(s), 1550(w), 1505(s), 1434(s), 1387(s), 1276(m), 1194(w), 1095(s), 848(w), 790(w), 739(m), 593(m), 491(w).

Results and discussion

Synthesis and structure analysis of *R-1/S-1* and *R-2/S-2*

We accurately weighed *R*-tartaric acid dihydrazide (0.1 mmol; 0.0178 g), 8-hydroxyquinoline-2-carboxaldehyde (0.2 mmol; 0.0346 g), and $\text{DyCl}_3\cdot 6\text{H}_2\text{O}$ (0.5 mmol; 0.1884 g), dissolved them in a mixed solvent of MeOH:MeCN (1.8:0.2 mL), and added 20 μL triethylamine. After evenly mixing, the mixture was reacted under heating conditions at 80 °C for 24 h to obtain yellow and red transparent mixed crystals, *R-1* and *R-2* (*R*-tartaric acid dihydrazide changed into *S*-tartaric acid dihydrazide and mixed crystals *S-1* and *S-2* were obtained (Scheme 2)). When other reaction conditions were kept constant and only the amount of metal salt was changed, pure yellow blocky crystals, *R-1* or *S-1*, were obtained. When the reaction raw materials were reduced by half under the same reaction conditions, pure red blocky crystals, *R-2* or *S-2*, were obtained.^{32–35} The results of single-crystal X-ray diffraction

(SCXRD) indicated that **R-1/S-1** crystallized in the $P2_12_12_1$ space group of the orthorhombic system (Table S1†). Because **R-1** and **S-1** are enantiomers of each other, only **R-1** was subjected to detailed structural analysis. The structural skeleton of **R-1** contains $2n$ Dy(III) ions, n -deprotonated R -(N^1E, N^4E)-2,3-dihydroxy- N^1, N^4 -bis((8-hydroxyquinolin-2-yl)methylene)succinohydrazide (R -(L^1) $^{2-}$) ligands, $3n$ -terminally coordinated Cl^- , $3n$ -coordinated CH_3OH molecules, n -free Cl^- , $4n$ -free CH_3OH molecules, n -free CH_3CN molecules and n -free H_2O molecules; its molecular formula is $[[Dy_2(R-L^1)(Cl)_3(CH_3OH)_3] \cdot Cl \cdot 4CH_3OH \cdot$

$CH_3CN \cdot 2H_2O]_n$ (Fig. 1). The smallest asymmetric unit of **R-1** contains two Dy(III) ions and a deprotonated R -(L^1) $^{2-}$ ligand molecule (Fig. 2a). The chiral ligand R -(L^1) $^{2-}$ in the **R-1** structure chelates two Dy(III) ions to form a template unit Dy_2L^1 with the same coordination point (*cis* template unit). This *cis* template unit is connected head-to-tail through coordination between the hydroxyl oxygen atom on the ligand quinoline ring and the Dy(III) ion, which continuously circulates and extends infinitely and eventually forms a 1D chain structure in which the template units are reversed, and exhibits an “S”-

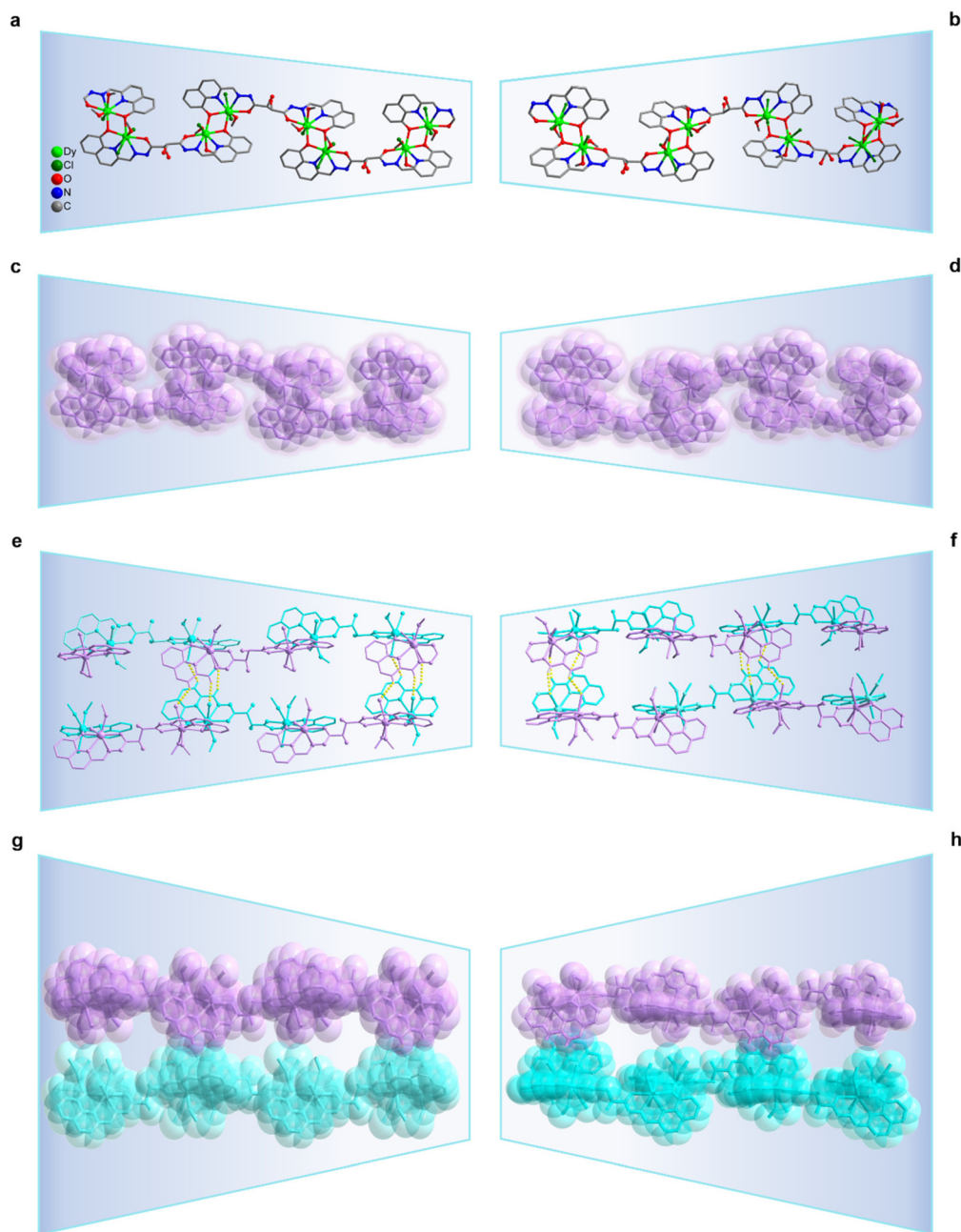


Fig. 1 One-dimensional (1D) chain structure of **R-1/S-1** (a and b), fill pattern diagram of **R-1/S-1** (c and d), secondary structure formed by hydrogen bonding connecting **R-1/S-1** chains (e and f), filling pattern diagram of the secondary structure of **R-1/S-1** (g and h).

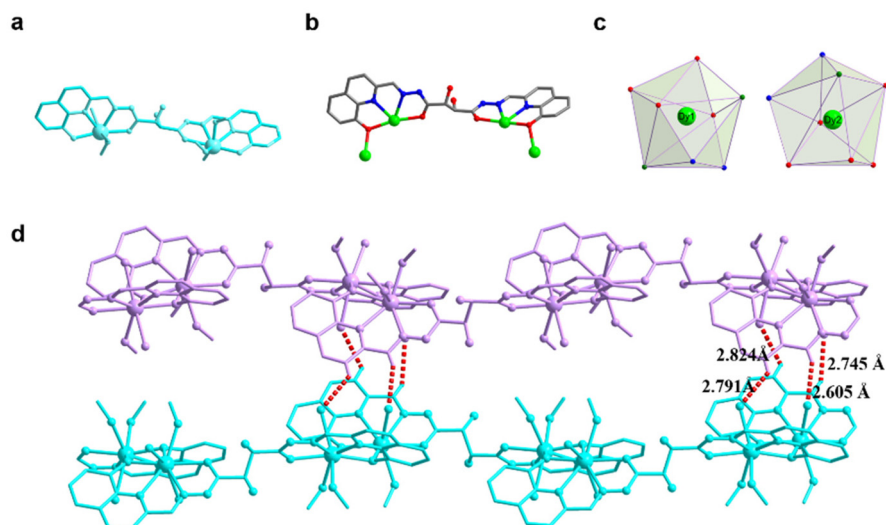


Fig. 2 The asymmetric unit of *R-1/S-1* (a), ligand coordination mode of clusters *R-1/S-1* (b), coordination polyhedron around the Dy(III) ions of *R-1/S-1* (c), *R-1* weak hydrogen bonding between chains (d).

shaped distribution (Fig. 1a and c). The two neighboring chains are connected through hydrogen bonds between the terminal-coordinated Cl^- and hydrogen atoms on the ligand to form a three-dimensional (3D) structure (Fig. 2d, 1e, and g). These hydrogen bonds are $\text{C11-H11}\cdots\text{Cl4}$ (2.791 Å), $\text{C15-H15}\cdots\text{Cl3}'$ (2.824 Å), $\text{C20-H20}\cdots\text{Cl4}'$ (2.745 Å), and $\text{C30-H30}\cdots\text{Cl3}'$ (2.605 Å) (Fig. 3g, 1e, and g). In addition, the coordination mode of the ligand $R\text{-}(L^1)^{2-}$ in complex *R-1* is $\mu_4\text{-}\eta^2\text{:}\eta^1\text{:}\eta^1\text{:}\eta^1\text{:}\eta^1\text{:}\eta^1\text{:}\eta^2$ (Fig. 2b). The metal centers Dy1 and Dy2 are in $\text{O}_4\text{N}_2\text{Cl}_2$ and $\text{O}_5\text{N}_2\text{Cl}$ coordination environments, respectively, formed by the ligand $R\text{-}(L^1)^{2-}$, coordinated anion Cl^- , and CH_3OH molecules (Fig. 2c). SHAPE calculations showed that the coordination configurations of the metal centers Dy1 and Dy2 were biaugmented trigonal prism (BTPR-8) with a C_{2v} symmetric environment (Table S6†). Structural analysis revealed that all Dy–O/N bond lengths in the structure of complex *R-1* were within the normal range (Table S2†).

Under the same reaction conditions, the reaction raw materials were reduced by half and subsequently the heating reaction was performed, obtaining only red blocky crystals, *R-2/S-2*. The SCXRD results revealed that *R-2/S-2* crystallized in the $P2_12_12_1$ space group of the orthorhombic system (Table S1†). Because *R-2* and *S-2* are enantiomers of each other, only *R-2* was subjected to detailed structural analysis. The structural skeleton of *R-2* contains $2n$ Dy(III) ions, n $R\text{-}(L^1)^{2-}$ ligands that remove two protons, $3n$ -terminally coordinated Cl^- , $2n$ -coordinated CH_3OH molecules, n -free Cl^- , n -free H_2O molecules and $4n$ -free CH_3OH molecules; its molecular formula is $[[\text{Dy}_2(\text{R-L}^1)(\text{Cl})_3(\text{CH}_3\text{OH})_2]\cdot\text{Cl}\cdot\text{H}_2\text{O}\cdot 4\text{CH}_3\text{OH}]_n$ (Fig. 3). Similarly, the smallest asymmetric unit of *R-2* contains two Dy(III) ions and one deprotonated $R\text{-}(L^1)^{2-}$ ligand molecule (Fig. 4a). In the structure of *R-2*, the twisted chiral ligand $R\text{-}(L^1)^{2-}$ chelates two Dy(III) ions in reverse coordination to form

a “*trans*” template unit Dy_2L^1 . In addition, multiple *trans* and twisted Dy_2L^1 template units are connected through coordination between the hydroxyl oxygen atom on the ligand quinoline ring and the Dy(III) ion, thereby forming a 1D chain with an axial helix (Fig. 3a and c). Notably, the coordination-driven self-assembly process of complex template units is considerably similar to the formation process of nucleic acids. The Dy_2L^1 template unit is similar to the base pairs in the DNA structure, possesses a certain orientation and recognition ability, and can specifically recognize other template units. This process is similar to the specific recognition of base pairs in the DNA sequence of organisms. For example, thymine T can specifically pair with adenine A and cytosine C can specifically pair with guanine G.^{36,37} The two chains are connected through the hydrogen bond interaction ($\text{N5-H5}\cdots\text{Cl3}$ (2.220 Å)) between the Cl^- and the hydrogen atom on $-\text{NH}-$ of the ligand to form a 3D structure (Fig. 4d, 3e, and g). In addition, the coordination mode of the ligand $R\text{-}(L^1)^{2-}$ in complex *R-2* is $\mu_4\text{-}\eta^2\text{:}\eta^1\text{:}\eta^1\text{:}\eta^1\text{:}\eta^1\text{:}\eta^1\text{:}\eta^2$ (Fig. 4b). The metal center Dy1 is in an $\text{O}_3\text{N}_2\text{Cl}_2$ coordination environment formed by the ligand $R\text{-}(L^1)^{2-}$ and coordinated Cl^- (Fig. 4c). SHAPE calculations revealed that the coordination configuration of the metal center Dy1 was a pentagonal bipyramid (PBPY-7) with a C_{2v} symmetric environment (Table S8†). The metal center Dy2 is in an $\text{O}_5\text{N}_2\text{Cl}$ coordination environment formed by the ligand $R\text{-}(L^1)^{2-}$, ligand Cl^- and CH_3OH molecule (Fig. 4c). SHAPE calculations revealed that the coordination configuration of the metal center Dy2 was BTPR-8 with a C_{2v} symmetric environment (Table S8†). Structural analysis revealed that all Dy–O/N bond lengths in the structure of complex *R-2* were within the normal range (Table S4†).

Herein, chiral template units with *cis* or *trans* configurations only selectively coordinate with template units having the same configuration during the coordination process. For

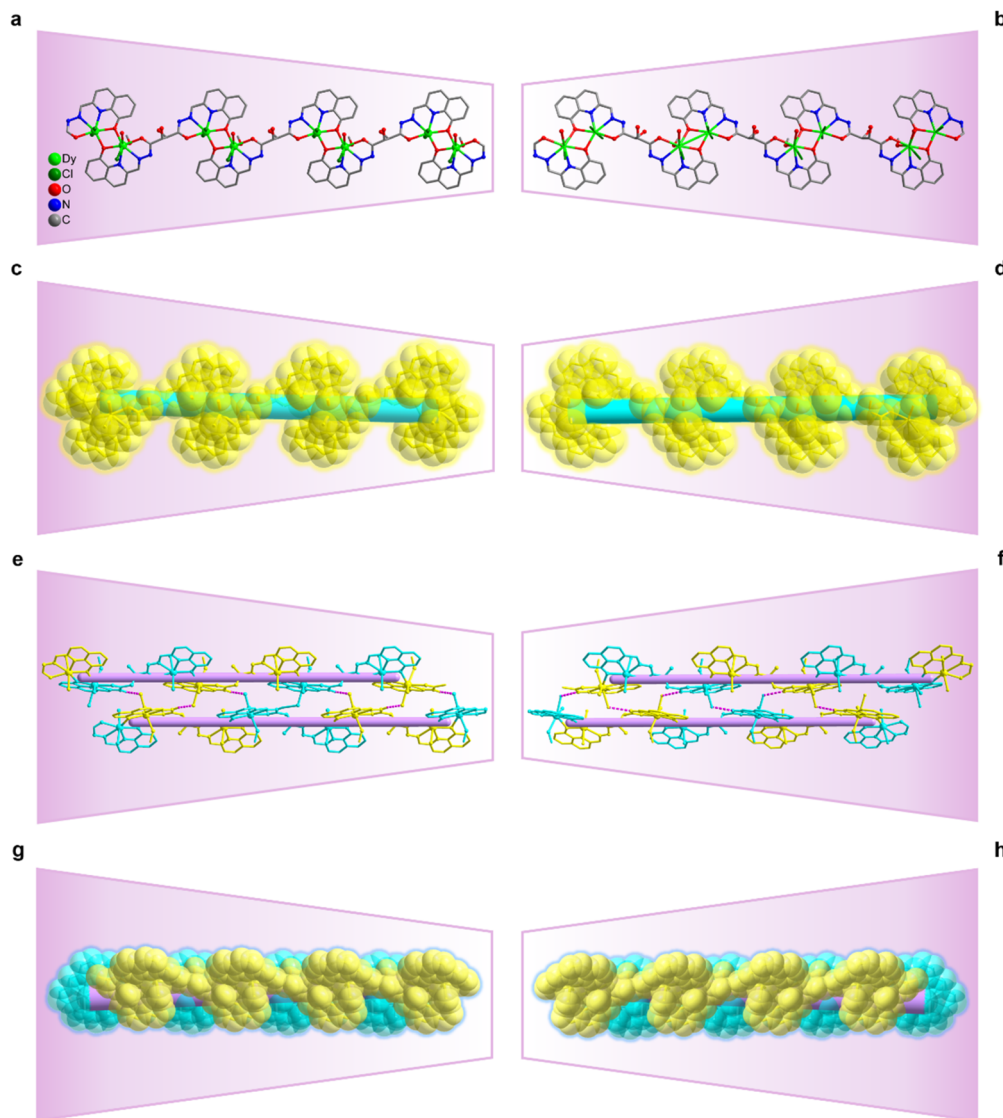


Fig. 3 One-dimensional (1D) spiral chain structure of *R-2/S-2* (a and b), fill pattern diagram of *R-2/S-2* (c and d), double helix structure formed by hydrogen bonding *R-2/S-2* (e and f), filling pattern diagram of the double helix structure of *R-2/S-2* (g and h).

the first time, supramolecular assembly has been used to simulate the specific recognition of base pairs in organisms to form DNA secondary structures.^{7,38} By regulating the proportion of the reaction raw materials in the “one-pot” synthesis process, we obtained a recognition function of the supramolecular self-assembly process to simulate the assembly mode of nucleotides. This reveals the adjustability of the lanthanide complex structure design and provides a new idea for constructing a molecular recognition model in biological systems.

R-1/S-1 and *R-2/S-2* are two pairs of enantiomers; thus, they have similar Fourier transform infrared absorption peaks. The results showed that a broad absorption peak at around 3300 cm^{-1} can be attributed to the stretching vibration of $\nu(\text{HO-H})$ in the H_2O molecule. The strong peaks around 1615 cm^{-1} can be attributed to the $\text{C}=\text{N}$ stretching vibration of the imine group ($-\text{C}=\text{N}-$). The strong peaks near 1450 cm^{-1}

can be attributed to the stretching vibration of $\text{C}=\text{N}$ and $\text{C}=\text{C}$ in the aromatic ring. The moderate intensity absorption peak around 1270 cm^{-1} can be attributed to the stretching vibration between $\text{C}-\text{O}$ of phenolic hydroxyl groups. The strong absorption peak appearing near 1090 cm^{-1} can be attributed to the stretching vibration between $\text{C}-\text{O}$ of alcoholic hydroxyl groups (Fig. S1†).³⁹ In addition, the simulated and observed values of powder X-ray diffraction values of *R-1/S-1* and *R-2/S-2* were compared at room temperature, and the results showed that they were both pure phases (Fig. S2†).

Circular dichroism spectra analysis of *R-1/S-1* and *R-2/S-2*

To verify the chiral optical activity and enantiomeric characteristics of *R-1/S-1* and *R-2/S-2*, we evaluated their CD spectra in a chromatographic-grade methanol solution. The CD signal peaks of the two enantiomers at a concentration of 0.1 g L^{-1} in

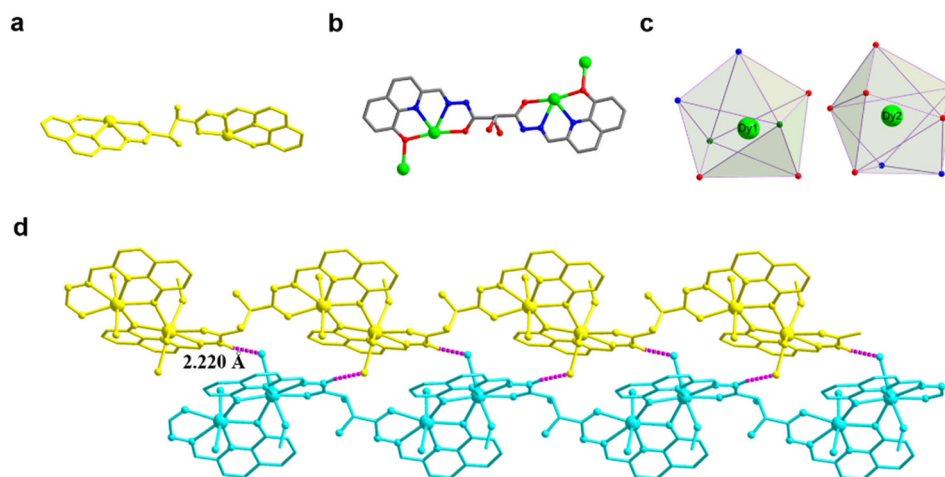


Fig. 4 The asymmetric unit of *R-2/S-2* (a), ligand coordination mode of clusters *R-2/S-2* (b), coordination polyhedron around the Dy(III) ions of *R-2/S-2* (c), *R-2* weak hydrogen bonding between chains (d).

the 200–500 nm range exhibited near-perfect mirror symmetry (Fig. 5b and d). The results indicated that the CD spectrum of *R-1* exhibited a positive Cotton effect with two peaks at 382 and 236 nm and a negative Cotton effect with three peaks at 355, 311, and 264 nm, whereas *S-1* exhibited opposite signals at the same positions, forming mirror symmetry. This indicates that *R-1* and *S-1* are a pair of enantiomers (Fig. 5b). The differences in structural connections yield slightly different CD spectra of *R-1/S-1* and *R-2/S-2*. The CD spectrum of *R-2* exhibi-

ted three peaks at 355, 312, and 263 nm showing a negative Cotton effect and three peaks at 386, 336, and 236 nm showing a positive Cotton effect, whereas *S-2* exhibited opposite signals at the same positions, which are mirror images of each other. This indicates that *R-2* and *S-2* are enantiomers of each other (Fig. 5d). Considering the ultraviolet absorption spectrum analysis, *R-1/S-1* and *R-2/S-2* exhibit weak and strong absorption peaks at 232 and 320 nm, respectively, attributed to the $n-\pi^*$ transition of the imine group and the $n-\pi^*$ and $\pi-\pi^*$

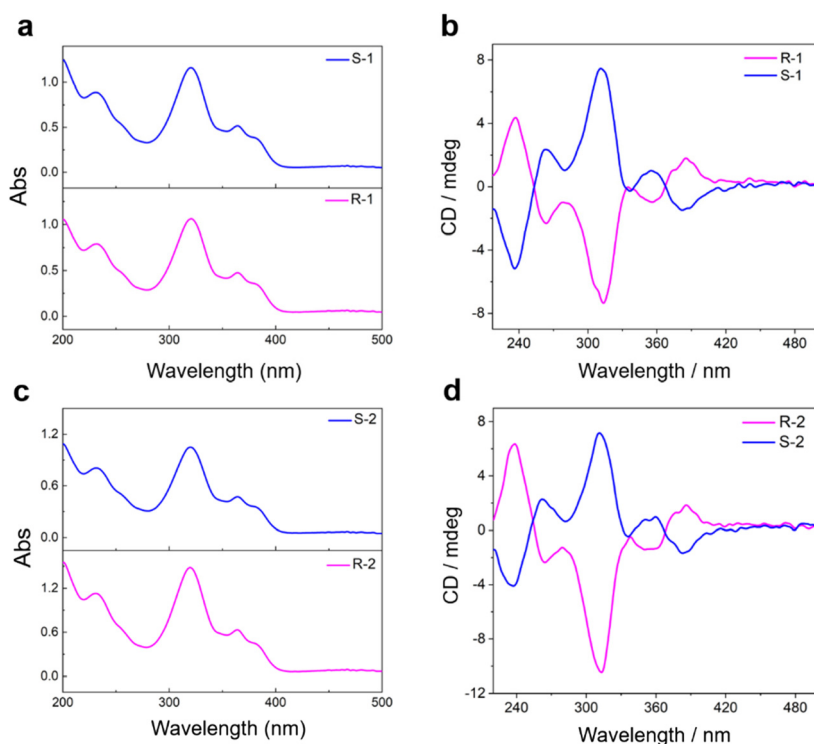


Fig. 5 The UV-vis absorption spectra of clusters *R-1/S-1* (a) and *R-2/S-2* (c); CD spectra of clusters *R-1/S-1* (b) and *R-2/S-2* (d).

transitions of the aromatic group on the ligand, whereas the appearance of a weaker absorption peak at 364 nm is attributed to the π - π^* transition of the ligand (Fig. 5a and c).^{18,19}

Magnetic analysis of *R-1/S-1* and *R-2/S-2*

Lanthanide metal ions with high spin, especially Dy(III) ions have large intrinsic magnetic anisotropy, are ideal 4f transition metal ions for constructing single-molecule magnets, often showing excellent energy barriers and relaxation time.⁴⁰ Therefore, we further studied the magnetic behavior of *R-1/S-1* and *R-2/S-2*. The temperature-varying molar susceptibilities of the *R-1/S-1* and *R-2/S-2* pure phases were tested under an external DC magnetic field of 1000 Oe in the 2–300 K temperature range (Fig. 6a, c, S4a, and S4c†).^{40–42} The $\chi_m T$ values of *R-1*, *S-1*, *R-2*, and *S-2* at 300 K were 28.24, 28.28, 28.39, and 28.30 cm³ K mol⁻¹, respectively (⁶ $H_{15/2}$, $S = 5/2$, $g = 4/3$, $J = 15/2$, and $L = 5$), which are close to the theoretical value (28.34 cm³ K mol⁻¹) of the two Dy(III) ions. When the temperature is gradually decreased to ~100 K, a slight decrease in $\chi_m T$ occurs for *R-1/S-1* and *R-2/S-2*. When the temperature decreases to 5 K, the $\chi_m T$ of *R-1* and *S-1* rapidly decreases to the minimum value of 22.92 and 22.37 cm³ K mol⁻¹, and then increases to 23.78 and 22.99 cm³ K mol⁻¹ at 2 K, respectively. The decrease in $\chi_m T$ in the 300–5 K temperature range may be caused by a decrease in the Stark sublevel of the Dy(III) ions excited state and/or the magnetic interaction, while its $\chi_m T$ value slightly increases in the 5–2 K temperature range. It may be caused by the weak ferromagnetic interaction between the metal centers in the system (Fig. 6a and S4a†). When the temperature approaches 2 K, the $\chi_m T$ values of *R-2/S-2* decrease rapidly and reach the minimum values of 21.83 and 21.79 cm³ K mol⁻¹,

respectively.^{43,44} These findings revealed that the temperature-decreasing $\chi_m T$ value may be caused by a decrease in the Stark sublevel of the Dy(III) ions excited state and the antiferromagnetic interaction (Fig. 6c and S4c†). In addition, we tested the field-dependent magnetization of *R-1/S-1* and *R-2/S-2* at different temperatures (2–5 K) and applied fields (0–7 T), and plotted the M vs. H/T curves (Fig. 6b, d, S4b, and S4d†). The measured magnetization at 2 K rapidly increased in the low-field region but gradually became flat in the high-field region. When reaching a static field of 13 kOe, *R-1*, *S-1*, *R-2*, and *S-2* reached maximum values of 11.38, 11.18, 12.01, and 11.94 $N\beta$, respectively. The M vs. H/T curves of *R-1/S-1* and *R-2/S-2* at different temperatures did not considerably overlap. The test results indicated that the Dy(III) ions may have low excited states or a large magnetic anisotropy. The hysteresis loops of *R-1/S-1* and *R-2/S-2* are not obvious at 2 K (Fig. S5†), which may be attributed to the existence of crystal field effects and strong quantum tunneling effects.

We further tested the alternating current (ac) magnetic susceptibility of *R-1/S-1* and *R-2/S-2* to explore their dynamic magnetic behavior. We observed that neither the *R-1/S-1* nor *R-2/S-2* in-of-phase (χ') and out-of-phase (χ'') signals exhibited an obvious frequency-dependent behavior under the zero DC field (Fig. S6 and S7†). When a certain external field is applied, the quantum tunneling effect may be suppressed. Therefore, *R-1* and *S-1* were tested for alternating current (ac) magnetic susceptibility under an external DC field of 1200 Oe and 800 Oe, respectively. The χ' and χ'' were plotted as functions of temperature (χ'/χ'' vs. T) and frequency (χ'/χ'' vs. ν), respectively (Fig. S8 and S9†). The results showed that both the in-of-phase (χ') and out-of-phase (χ'') signals of *R-1* and *S-1* exhibited temp-

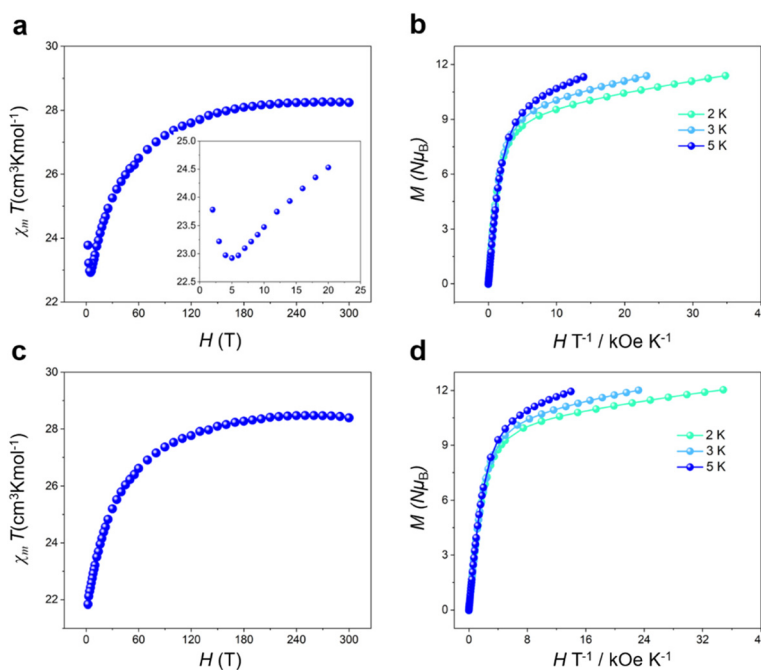


Fig. 6 Temperature dependence of $\chi_m T$ for *R-1* (a) and *R-2* (c); M vs. H/T plots of *R-1* (b) and *R-2* (d).

erature and frequency-dependent behavior, proving that **R-1** and **S-1** have slow magnetic relaxation behavior. Similarly, **R-2** and **S-2** were tested for alternating current (ac) magnetic susceptibility under an external DC field of 1000 Oe and 800 Oe, respectively. The χ' and χ'' were plotted as functions of temperature (χ'/χ'' vs. T) and frequency (χ'/χ'' vs. ν), respectively (Fig. S8 and S9†). The results showed that both the in-of-phase (χ') and out-of-phase (χ'') signals of **R-2** and **S-2** exhibited temperature and frequency-dependent behavior, but no peak was observed, proving that **R-2** and **S-2** have slow magnetic relaxation behavior.

Conclusions

We regulate the ratio of reaction materials in the “one-pot” synthesis of lanthanide complexes to form chiral template units with coordination sites in *cis* or *trans* configurations and further undergo self-assembly through a coordination-driven recognition process to obtain a chiral 1D chain isomer with an “S”-shaped distribution, **R-1/S-1**, and a chiral helix chain, **R-2/S-2**. The *cis* or *trans* configuration chiral template unit selectively further self-assembles with a template unit of the same configuration during coordination recognition to generate differential chiral 1D lanthanide chains. To the best of our knowledge, this is the first study to construct chiral lanthanide complexes with different linkages through the self-recognition of template units with different configurations through the self-assembly process of coordination recognition. In living systems, chiral macromolecules are usually formed from simple chiral units that undergo complex reaction processes. The coordination-driven recognition process in this study provides a new approach to simplify and simulate the formation of complex chiral macromolecules with multilevel structures (such as nucleic acids and proteins) from simple primitives (such as nucleotides and amino acids) in living organisms. Moreover, this work will advance the crystal engineering of lanthanide complexes with different structural connections and is expected to achieve precise directional and controllable synthesis of lanthanide complexes.

Conflicts of interest

There are no conflicts to declare.

Acknowledgements

This work was supported by the National Natural Science Foundation of China (22271068, 22075058, and 22061005).

References

- P. Peluso and B. Chankvetadze, *Chem. Rev.*, 2022, **122**, 13235–13400.
- D. P. Glavin, A. S. Burton, J. E. Elsila, J. C. Aponte and J. P. Dworkin, *Chem. Rev.*, 2020, **120**, 4660–4689.
- J. Liu, S. Mukherjee, F. Wang, R. A. Fischer and J. Zhang, *Chem. Soc. Rev.*, 2021, **50**, 5706–5745.
- G. Kong, M. Xiong, L. Liu, L. Hu, H. M. Meng, G. Ke, X. B. Zhang and W. Tan, *Chem. Soc. Rev.*, 2021, **50**, 1846–1873.
- A. F. De Fazio, D. Misatziou, Y. R. Baker, O. L. Muskens, T. Brown and A. G. Kanaras, *Chem. Soc. Rev.*, 2021, **50**, 13410–13440.
- M. Xiao, W. Lai, T. Man, B. Chang, L. Li, A. R. Chandrasekaran and H. Pei, *Chem. Rev.*, 2019, **119**, 11631–11717.
- J. D. Watson and F. H. C. Crick, *Nature*, 1953, **171**, 737–738.
- S. Akine and H. Miyake, *Coord. Chem. Rev.*, 2022, **468**, 214582.
- S. J. Bradberry, A. J. Savyasachi, M. Martinez-Calvo and T. Gunnlaugsson, *Coord. Chem. Rev.*, 2014, **273–274**, 226–241.
- X. Z. Li, C. Bin Tian and Q. F. Sun, *Chem. Rev.*, 2022, **122**, 6374–6458.
- R. Carr, N. H. Evans and D. Parker, *Chem. Soc. Rev.*, 2012, **41**, 7673.
- H.-Y. Wong, W.-S. Lo, K.-H. Yim and G.-L. Law, *Chem*, 2019, **5**, 3058–3095.
- Y. Li, M. Zhou, Y. Song, T. Higaki, H. Wang and R. Jin, *Nature*, 2021, **594**, 380–384.
- X.-Q. Guo, L.-P. Zhou, S.-J. Hu, L.-X. Cai, P.-M. Cheng and Q.-F. Sun, *J. Am. Chem. Soc.*, 2021, **143**, 6202–6210.
- S. Li, X. S. Du, B. Li, J. Y. Wang, G. P. Li, G. G. Gao and S. Q. Zang, *J. Am. Chem. Soc.*, 2018, **140**, 594–597.
- M. H. Du, S. H. Xu, G. J. Li, H. Xu, Y. Lin, W. D. Liu, L. S. Long, L. S. Zheng and X. J. Kong, *Angew. Chem., Int. Ed.*, 2022, **61**, e202116296.
- C.-Y. Li, H. Xu, P.-M. Cheng, M.-H. Du, L.-S. Long, L.-S. Zheng and X.-J. Kong, *J. Am. Chem. Soc.*, 2023, **145**, 22176–22183.
- B. F. Long, S. Yu, Z. H. Zhu, Y. L. Li, F. P. Liang and H. H. Zou, *Inorg. Chem. Front.*, 2022, **9**, 5950–5959.
- B. F. Long, Y. L. Li, Z. H. Zhu, H. L. Wang, F. P. Liang and H. H. Zou, *Dalton Trans.*, 2022, **416**, 17040–17049.
- Y. Liu, Y. Liu and S. Zang, *Angew. Chem., Int. Ed.*, 2023, **62**, e202311572.
- C. Tan, J. Jiao, Z. Li, Y. Liu, X. Han and Y. Cui, *Angew. Chem., Int. Ed.*, 2018, **57**, 2085–2090.
- M. Feng, B. H. Lyu, M. H. Wang, W. W. Wu, Y. C. Chen, G. Z. Huang, W. Q. Lin, S. G. Wu, J. L. Liu and M. L. Tong, *Inorg. Chem.*, 2019, **58**, 10694–10703.
- Y. L. Li, H. L. Wang, Z. H. Zhu, F. P. Liang and H. H. Zou, *Coord. Chem. Rev.*, 2023, **493**, 215322.
- Z. H. Zhu, X. F. Ma, H. L. Wang, H. H. Zou, K. Q. Mo, Y. Q. Zhang, Q. Z. Yang, B. Li and F. P. Liang, *Inorg. Chem. Front.*, 2018, **5**, 3155–3162.
- H. L. Wang, T. Liu, Z. H. Zhu, J. M. Peng, H. H. Zou and F. P. Liang, *Inorg. Chem. Front.*, 2021, **8**, 2136–2143.

- 26 W.-W. Qin, Y.-L. Li, Z.-H. Zhu, F.-P. Liang, Q. Hu and H.-H. Zou, *Inorg. Chem. Front.*, 2023, **10**, 6269–6281.
- 27 Y.-L. Li, W.-W. Qin, H.-L. Wang, Z.-H. Zhu, F.-P. Liang and H.-H. Zou, *Inorg. Chem. Front.*, 2023, **10**, 5337–5346.
- 28 Z. R. Luo, H. L. Wang, Z. H. Zhu, T. Liu, X. F. Ma, H. F. Wang, H. H. Zou and F. P. Liang, *Commun. Chem.*, 2020, **3**, 1–9.
- 29 Z. H. Zhu, J. M. Peng, H. L. Wang, H. H. Zou and F. P. Liang, *Cell Rep. Phys. Sci.*, 2020, **1**, 100165.
- 30 Y.-L. Li, H.-L. Wang, Z.-H. Zhu, F.-P. Liang and H.-H. Zou, *Inorg. Chem.*, 2022, **61**, 10101–10107.
- 31 H. L. Wang, X. F. Ma, J. M. Peng, Z. H. Zhu, B. Li, H. H. Zou and F. P. Liang, *Inorg. Chem.*, 2019, **58**, 9169–9174.
- 32 F.-H. Zhao, Z.-L. Li, Y.-H. Yu, S.-Y. Fan, X.-W. Guo and Z.-H. Zhao, *J. Cluster Sci.*, 2021, **32**, 45–54.
- 33 S. Hiraoka, T. Yi, M. Shiro and M. Shionoya, *J. Am. Chem. Soc.*, 2002, **124**, 14510–14511.
- 34 M. N. Akhtar, X.-F. Liao, Y.-C. Chen, J.-L. Liu and M.-L. Tong, *Dalton Trans.*, 2017, **46**, 2981–2987.
- 35 Z. Pang, N. Ren, Y. Wu, J. Qi, F. Hu, Y. Guo, Y. Xie, D. Zhou and X. Jiang, *Adv. Mater.*, 2023, **35**, 1–18.
- 36 M. Cobb and N. Comfort, *Nature*, 2023, **616**, 657–660.
- 37 M. H. F. Wilkins, A. R. Stokes and H. R. Wilson, *Nature*, 1953, **171**, 738–740.
- 38 M. Liu, Y. He, C. Shan, L. Wojtas, I. Ghiviriga, O. Fathalla, Y. Yan, X. Li and X. Shi, *Chem. Sci.*, 2021, **12**, 7569–7574.
- 39 H.-L. Wang, T. Liu, Z.-H. Zhu, J.-M. Peng, H.-H. Zou and F.-P. Liang, *Inorg. Chem. Front.*, 2021, **8**, 3134–3140.
- 40 J. Liu, Y. C. Chen, J. L. Liu, V. Vieru, L. Ungur, J. H. Jia, L. F. Chibotaru, Y. Lan, W. Wernsdorfer, S. Gao, X. M. Chen and M. L. Tong, *J. Am. Chem. Soc.*, 2016, **138**, 5441–5450.
- 41 Z. Zhu, C. Zhao, T. Feng, X. Liu, X. Ying, X. L. Li, Y. Q. Zhang and J. Tang, *J. Am. Chem. Soc.*, 2021, **143**, 10077–10082.
- 42 P. Zhang, L. Zhang, C. Wang, S. Xue, S. Y. Lin and J. Tang, *J. Am. Chem. Soc.*, 2014, **136**, 4484–4487.
- 43 J. L. Liu, Y. C. Chen and M. L. Tong, *Chem. Soc. Rev.*, 2018, **47**, 2431–2453.
- 44 Y. C. Chen, J. L. Liu, L. Ungur, J. Liu, Q. W. Li, L. F. Wang, Z. P. Ni, L. F. Chibotaru, X. M. Chen and M. L. Tong, *J. Am. Chem. Soc.*, 2016, **138**, 2829–2837.